Faraday Discussions

Cite this: *Faraday Discuss.*, 2024, **249**, 424

PAPER

Collective motion of Nafion-based micromotors in water†

Jordi Fraxedas, *[a] David Reguera [b] and María José Esplandiu [a]

Received 15th May 2023, Accepted 10th July 2023
DOI: 10.1039/d3fd00098b

Ion exchange is one of the most interesting processes occurring at the interface between aqueous solutions and polymers, such as the well-known Nafion. If the exchanged ions have different diffusion coefficients, this interchange generates local electric fields which can be harnessed to drive fluid motion. In this work, we show how it is possible to design and fabricate self-propelling microswimmers based on Nafion, driven by ion-exchange, and fueled by innocuous salts. These Nafion micromotors are made using colloidal lithography by micro/nanostructuring Nafion in the form of asymmetric rods. These microswimmers exhibit fascinating collective motion in water driven by the interplay of their self-generated chemical/electric fields and their capability to pump matter nearby towards the collective motile structure. The pumping activity of the microswimmers induces the formation of growing mobile clusters, whose velocity increases with size. Such dynamic structures are able to trap nearby micro/nano-objects while purifying the liquid, which acts both as the transport media and as fuel. Such phenomenology opens the door to potential applications in water remediation that are currently under development.

1. Introduction

The field of nanoscience and nanotechnology has grown rapidly over the last few decades, with researchers seeking to harness the unique properties of materials and systems at the nanoscale. One of the most promising areas of research in this field is the development of self-powered machines that can move in a fluid environment in a controlled and autonomous way while performing specific tasks. This technology has the potential to provide innovative solutions, especially in the fields of medicine, environmental monitoring and remediation, and energy conversion.[1–8] For example, these self-powered micromachines can be used as

[a]*Catalan Institute of Nanoscience and Nanotechnology (ICN2), CSIC and BIST, Campus UAB, Bellaterra, 08193 Barcelona, Spain. E-mail: jordi.fraxedas@icn2.cat*

[b]*Departament de Física de la Matèria Condensada and Institute of Complex Systems (UBICS), Universitat de Barcelona, C/Martí i Franquès 1, 08028, Barcelona, Spain*

† Electronic supplementary information (ESI) available: Video showing collective motion of Nafion microswimmers. See DOI: https://doi.org/10.1039/d3fd00098b

drug delivery vehicles, as they can be guided to specific locations within the body and deliver therapeutic agents with high precision or used as *in vivo* sensing/imaging agents.[9,10] They can also be used in lab-on-a-chip devices for capture, transport, delivery, separation, and sensing of bioanalytes;[9,11,12] for detecting pollutants or for trapping and degrading contaminants from water.[6–8] Additionally, self-powered machines can be used to convert different kinds of energies into mechanical work, which can be harnessed to power various devices. Moreover, these micro/nanomachines have revolutionized the field of active matter through their capabilities of exhibiting collective/cooperative behaviors. This can lead to the emergence of complex and fascinating phenomena, such as pattern formation, swarming behavior, and motion synchronization, similar to natural active matter systems, such as swarms of bacteria or schools of fish.[13–21]

In this context, many self-powered devices have been developed. Among them, those that are self-propelled by chemical means have attracted considerable attention.[1,2,11] To confer motility capabilities to chemically driven micro/nanostructures, they should be designed with some sort of anisotropy, *e.g.* in material composition, shape or reactivity. Such anisotropy should guarantee asymmetric reactions that generate interfacial chemical gradients (which, for charged species, result also in the generation of local electric fields), triggering diffusio-osmotic or electrokinetic phenomena that can ultimately induce interfacial fluid motion.[1,2] If the object is dispersed in a fluid, the interfacial chemical gradients and resulting interfacial fluid flow should make the object behave as a micro/nanomotor or swimmer. If the object is immobilized, it acts as a pump, moving the fluid around. In this respect, both swimmers and pumps share the same operational principles.[22–26] In some cases, the chemical reaction at the motor surface produces gaseous products that can nucleate into micron-sized bubbles, inducing motion through an alternative mechanism to electrokinetic or diffusio-osmosis.[27] In this case, the detachment of bubbles from the micro-/nanomotor's surface produces a recoil force to thrust the movement of the motors.

However, one of the main limitations of these devices is that they are triggered by non-innocuous chemicals (*e.g.*, H_2O_2), which prevents their applicability in various environments. In addition, most mechanisms cannot work at high salt concentrations typical of biological systems. Among the different mechanisms explored to achieve chemical self-propulsion, ion exchange has emerged as a valuable strategy with the significant advantage of using innocuous salts as fuels and being able to work at biologically relevant conditions.[28]

Under this context, one of the most promising ion exchanger polymers is Nafion. Nafion is made up of a backbone of perfluorinated carbon atoms with pendant sulfonic acid groups ($-SO_3H$). These sulfonic acid groups are responsible for the ion-exchange properties of Nafion. They are highly polar and attract cations such as protons or metal ions while repelling anions. Due to its high affinity for protons, Nafion has become an excellent material for fuel cells, where it is used as a proton exchange membrane to generate electricity. Nafion is also used in ion-exchange chromatography to separate and purify molecules based on their charge, in sensors as a biocompatible membrane for detecting specific ions or molecules, and as an antifouling material, among other applications.[29]

Nafion has been considered a peculiar material and has been the subject of a controversial and long-standing debate due to its ability to form a solute

exclusion zone (EZ) of hundreds of microns in contact with water.[30–32] Motivated by the lack of understanding about this aspect of Nafion, our group has delved into the characterization of this phenomenon in connection with its ion-exchange properties.[33] In previous studies, we demonstrated that such a long-range EZ is mainly due to the presence of a built-up electric field pointing normally to the Nafion surface. This electric field arises from the unequal diffusion coefficients of the exchanged ions, which sets up an ion gradient. Such an electric field expels many solutes in water away from the Nafion interface, which also explains its attributes as an antifouling material.[33]

The Nafion interface and the ion-exchange mechanism provide the essential ingredients to generate fluid motion: chemical gradients and electric fields. However, to accomplish that, it is important to have a component of the electric field tangential to the interface. One way to achieve this is by micro/nanostructuration. Therefore, in this work, we will address the nanofabrication and characterization of micro/nanomachines based on Nafion. We will support our findings with numerical simulations, demonstrating that individual asymmetric Nafion nanostructures can move within the bulk liquid independently of the influence of charged walls. Additionally, we will showcase how these individual Nafion structures can self-assemble while swimming, leading to the emergence of collective behaviors.

The structure of the paper will consist of two main parts. First, we will provide a brief summary of the capabilities of Nafion pumps, alluding to previous studies in our group, which set the basis for understanding the mechanism of motion of Nafion-based swimmers. In the second part, we present a simple design of Nafion microswimmers and illustrate with simulations their ability to self-propel in water. We will then introduce a versatile nanofabrication strategy for developing Nafion micro/nanoswimmers and subsequently evaluate their ability to facilitate the emergence of collective behaviors.

2. Results and discussion

2.1 Nafion-based micropumps

The best platforms to design and understand the operational mechanisms of Nafion-based swimmers are Nafion pumps, their immobilized counterparts. Nafion micropumps can be fabricated using different strategies. One strategy consists of patterning thin Nafion membranes onto a support, such as gold-modified silicon wafers, using electron beam lithography (EBL). The electron beam efficiently deactivates Nafion by damaging its chemical integrity which allows for the definition of Nafion structures in various sizes and shapes (see Fig. 1a).

Another approach involves the previous patterning of gold structures onto a SiO_2 wafer again using EBL and then the spin coating of a Nafion layer on top. Nafion binds weakly to SiO_2 due to the strong negative charge between SiO_2 and Nafion but it binds more strongly to Au. An ultrasonic bath in water can then selectively remove the Nafion layer on SiO_2 surfaces, leaving only the coating on the Au patterns (see Fig. 1b).

These Nafion micropumps can be used to promote radial and, by proper microstructuring, also unidirectional fluid pumping.[28] Fig. 1a and b show typical Nafion patterns (discs or rectangles) that induce an inward fluid pumping.

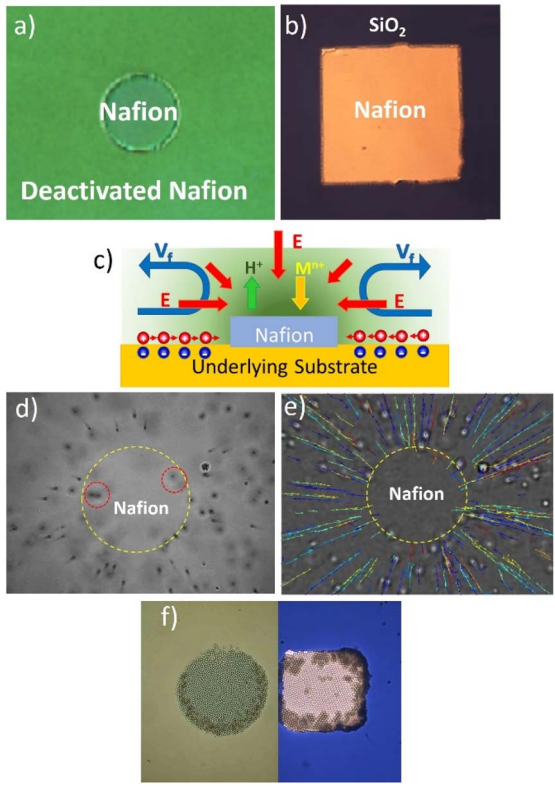

Fig. 1 (a) and (b) Different ways of patterning Nafion films, either (a) by direct electron beam lithography on Nafion films (deactivated Nafion) or (b) by first defining gold micropatterns by electron beam lithography, then Nafion deposition on the micro-patterned support and subsequent selective removal of Nafion layers by ultrasonic bath in water solutions. (c) Scheme illustrating the generation of fluid flow by ion-exchange. Protons are released whereas metal cations are trapped by Nafion. The different mobility of the exchanged cations generates a concentration gradient and an electric field pointing towards the Nafion. The micropatterning generates a tangential component of the electric field which drags fluid towards the Nafion pattern promoted by the negative zeta potential of the surface surrounding the Nafion structure. (d) Visualization of the fluid flow using microparticles as tracers. The particles move towards the Nafion disc and then lift up due to fluid continuity (see the enclosed particles in dashed red lines which become out of focus when are lifted up). (e) Particle trajectories towards the disc. (f) SiO_2 microparticles which have been transported to the Nafion pattern and form a local self-assembled layer of particles on top of Nafion.

Previously, we referred to the generation of a perpendicular electric field towards Nafion during the ion exchange process. The micropatterning of Nafion allows for the formation of a tangential component of the electric field, which is crucial for the activation of interfacial fluid flows. The surroundings of Nafion patterns, either deactivated Nafion or SiO_2, exhibit a negative zeta potential ($\zeta_{\text{deact. Nafion}} = -37$ mV, $\zeta_{SiO_2} = -66$ mV), which builds up a positive counterions region at the liquid interface.[28] The presence of the tangential electric field pointing to the Nafion moves the positive counterions toward the polymer dragging the fluid

along and generating a fluid flow. Due to the fluid continuity, the fluid flows lift up at the center of the micropatterned Nafion structure generating convective rolls. Fig. 1c schematizes the pumping mechanism driven by ion-exchange. The fluid pumping can be visualized by tracking polystyrene microparticles of quasi-neutral zeta potential ($\zeta = -12$ mV). Fig. 1e shows the particle motion towards the center of a Nafion disc together with the microparticle trajectories. In this case, the fluid pumping has been activated when the patterned Nafion system is immersed in 1.0×10^{-4} M NaCl solutions due to the exchange of protons by the salt cations. Particles close to the surface move toward the Nafion disc, however, as they approach the disc edge their trajectories bend upward in the direction perpendicular to the disc (see particles enclosed in a dashed red circle) and finally bend outward from the disc due to fluid continuity. The pump performance is evaluated by tracking the average radial velocities of the polystyrene tracers dispersed in NaCl at the region close to the surface (Fig. 1d). Maximum radial velocities above 20 μm s^{-1} have been monitored under these conditions, but such values can be modulated with the type of salt, concentration, and operation time.

Long-range unidirectional fluid pumping can be also achieved by fine-tuning the zeta potentials surrounding the active Nafion.[28] With proper

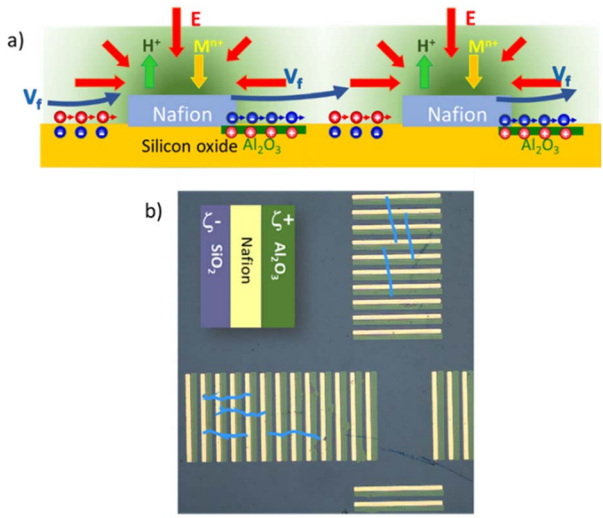

Fig. 2 (a) Scheme of a unidirectional pump based on the periodic repetition of a basic unit made of alternating strips of SiO_2 (negative ζ)/Nafion/Al_2O_3 (positive ζ) which would lead to unidirectional fluid flow along the patterned surface. The charged interface in the Nafion has been omitted to simplify the content of the figure. The interaction of the tangential electric field with the negative zeta potential of SiO_2 (at the left side of Nafion) will move the positive counterions accumulated at the SiO_2 interface dragging a fluid flow towards Nafion. In turn the Al_2O_3 patches (at the right side of Nafion) with positive ζ accumulate negative counterions that in the presence of the tangential component of the electric field will move the negative counterions to the right, dragging the fluid along to the next repeating unit, thus achieving unidirectional flow. (b) Patterned array of strips forming a cross made from the repetitive unit SiO_2/Nafion/Al_2O_3 as indicated in the inset. Such a pattern induces orthogonal fluid flows as can be visualized by the particle tracer trajectories (blue lines).

nanofabrication strategies, one can create an array of Nafion microstrips integrated into an array of adjoining strips with alternating positive/negative zeta potentials. Fig. 2a shows a scheme of an array of strips made from the periodic unit composed of SiO_2 (25 μm, $\zeta = -66$ mV)/Nafion (25 μm, $\zeta = -73$ mV)/Al_2O_3 (30 μm, $\zeta = 17$ mV).[28] The SiO_2 strip on the left side of the Nafion pad will induce fluid flows in the direction of Nafion, as in the case of the radial pump. The introduction of a positive zeta potential strip on the right side of Nafion (Al_2O_3) will break the surface charge symmetry around Nafion by building up negative counterions at the liquid interface. The electric field pointing towards Nafion will move the negative counterions at the Al_2O_3 interface in the opposite direction, producing an electro-osmotic fluid flow in the opposite direction, that is towards the next strips of silicon oxide and Nafion. Therefore, by periodically repeating a basic structure formed by alternating strips of negative ζ/Nafion/positive ζ the convective rolls are suppressed, driving a net fluid flow in one direction. Such nanofabricated arrays can be patterned with different orientations thus adding versatility to manipulate fluids at will. For instance, Fig. 2b shows patterned arrays in a cross-like fashion, which allows the generation of orthogonal fluid flows. The figure depicts some microparticle trajectories (light blue lines) which visualize such orthogonal fluid flows.[28]

Nafion-based pumps have many potential applications and have opened new possibilities in the area of wireless micro/nanofluidic networks. They can guide fluid flows and induce transport, accumulation, self-assembly, or clearance of matter in precise locations, making them useful in applications such as water decontamination, drug delivery, and biosensing. Previous studies in our group have used these pumps for the selective removal of cadmium ions from water samples in very short operation times.[28] Remarkably, the cadmium contaminant itself acts as fuel to drive the fluid pumping. They have also been used for accumulation and self-assembling matter in precise locations, as illustrated in this case with the self-assembly of silica microparticles in Fig. 1f. The fluid flow has been used to drag particles to the Nafion disc and induce their accumulation in a periodic structure on top of the Nafion disc.

2.2 Nafion micro/nanoswimmers

The previous results with pumps have encouraged us to develop Nafion-based microswimmers in order to exploit other functionalities. Interestingly, previous studies have used other ion-exchange materials, such as Amberlite microparticles, to form complexes with the ability to swim. Motion only occurs when these ion-exchange particles interact with other passive particles to form asymmetric modular complexes without being attached to each other.[34–36] None of the constituents have shown any active swimming by themselves. It has been observed that the swimming speed increased stepwise upon increasing the number of passive particles and then saturated at a moderate maximum speed below 6 μm s^{-1}.[35] The modular motion has been explained by the electric field generated by the ion-exchange resin, which induces an electro-osmotic solvent flow on the charged substrate or walls of the cell containing the particle dispersion. Recently, another study has addressed the use of sulfonated polystyrene beads as ion exchangers forming microbead complexes with ZnO rods to demonstrate active swarm complexes.[37]

2.2.1 Simulations. As anticipated, one of the main requirements for self-propelling swimmers is compositional or shape asymmetry, in order to guarantee asymmetric chemical gradients and activate phoretic mechanisms. In this context, a desirable aspect to go beyond previous ion-exchange swimmers is the integration of the required asymmetry in the swimmer itself without the need for adding other passive particles to trigger net motion. An asymmetric ion-exchange motor will have the capability to self-propel in bulk and will not require the proximity/presence of walls to move. Accordingly, finite element simulations have been performed to evaluate the self-propulsion capability of a simple design of an asymmetric Nafion-based micromotor. The simulations, similar to those performed in ref. 28 and 33, have been implemented using the software COMSOL Multiphysics v4.3, which solves the system of coupled Poisson's

$$-\varepsilon\nabla^2\varphi = \rho_e, \tag{1}$$

Stokes'

$$\nabla\cdot\boldsymbol{\nu} = 0 \text{ and } \eta\nabla^2\boldsymbol{\nu} = \nabla p + \rho_e\nabla\varphi \tag{2}$$

and Nernst–Planck's

$$\boldsymbol{\nu}\cdot\nabla C_i = \nabla\cdot(D_i\nabla C_i + z_iF\mu_i\nabla\varphi C_i) \tag{3}$$

differential equations and a first order ion-exchange reaction at the Nafion interface:

$$j_{ie} = k_{ie}[Na^+] \tag{4}$$

with a rate constant $k_{ie} = 10^{-4}$ m s^{-1}, governing the system behaviour. The Poisson's equation relates the local charge density $\rho_e = \sum_i Fz_iC_i$ with the electrostatic potential φ, where ε $(= \varepsilon_r\varepsilon_0)$ represents the permittivity of the liquid, F is Faraday's constant and C_i and Z_i stand for the molar concentration and the valence of each ionic species, respectively, designated by the subscript i. The stationary Stokes' equations describe the motion of an incompressible fluid at low Reynolds numbers, where $\boldsymbol{\nu}$, p and η represent the fluid velocity, pressure and viscosity, respectively. Finally, the stationary Nernst–Planck's equation for mass transport includes the diffusion coefficient D_i and the mobility of the different species μ_i. The mobility is connected to the diffusion coefficient through Einstein's relation, $D_i = \mu_iRT$, where R is the ideal gas constant and T is the absolute temperature.

Profiting from the symmetry of the system, a 2D axisymmetric domain of bulk water of 10 μm radius and 20 μm length at pH 7.0 and with a salt concentration of 10^{-5} M of NaCl has been simulated. Mimicking the experimental shape described in the next section, as a model system we implemented a Nafion rod of 0.75 μm radius, 2.2 μm length, and zeta potential −35 mV capped with a passive, positively charged bead of 1.8 μm diameter and zeta potential +17 mV. We also simulated a Nafion cylinder without the capping sphere. In both cases, the simulations are done in the reference system of the Nafion structure with stick boundary conditions and open upper and lower boundaries of the water domain. Zero ionic flux is

imposed on the passive bead and to avoid charge accumulation and to maintain steady-state conditions, the rate of protons released by the Nafion into the solution must be the same as the rate of uptaken salt cations (Na^+ in our case) at the Nafion interface. The concentration of all ions is fixed at the boundaries of the bulk water domain, where the electrostatic potential is also fixed to $\varphi = 0$. The system was meshed with 33 204 triangular elements with 100 boundary layers. A mesh sensitivity analysis was performed that guaranteed that the error in the estimated motor velocity was below 5%. Additional parameters used in the simulation were: diffusion coefficients of H^+, OH^-, Cl^-, and Na^+ are 9.31×10^{-9} m^2 s^{-1}, 5.28×10^{-9} m^2 s^{-1}, 2.03×10^{-9} m^2 s^{-1}, and 1.33×10^{-9} m^2 s^{-1}, respectively, temperature $T = 298$ K, relative permittivity of water $\varepsilon_r = 78$, density $= 10^3$ kg m^{-3} and dynamic viscosity $= 10^{-3}$ Pa s. Due to the exchange of

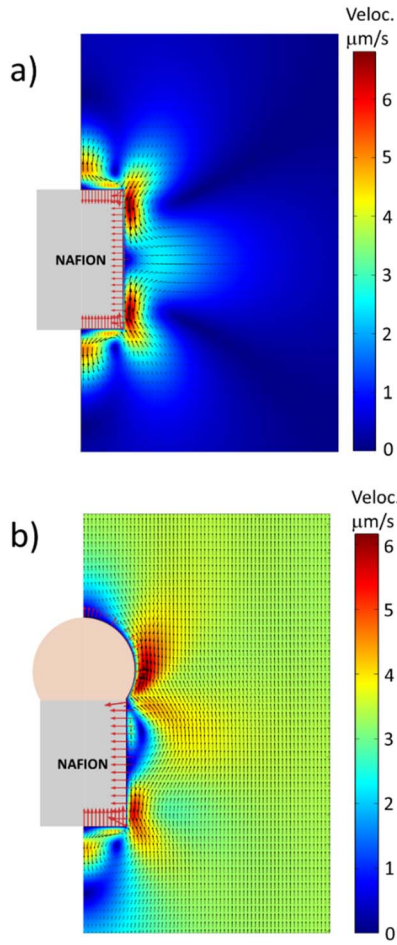

Fig. 3 Numerical simulations for (a) a Nafion rod and (b) a Nafion rod capped by a passive sphere. The figure shows the electric field (red arrows) and the stationary velocity field (black arrows), plotted in the reference system of the Nafion. The colour scale represents the magnitude of the velocity.

ions with different diffusion coefficients, a concentration gradient and an electric field are spontaneously built-up near the Nafion interface, as mentioned before.

Fig. 3 shows the fluid velocity and electric field obtained from the simulations in the vicinity of the two different Nafion microstructures: (a) a Nafion cylinder and (b) a Nafion cylinder capped with a passive particle (*i.e.*, not capable of ion exchange). In the first case, the Nafion cylinder generates local recirculation flows near its lateral surface. But the fluid velocity far from the cylinder is zero, indicating that this symmetric system is not able to move with a net velocity. Contrarily, when the Nafion rod is capped by a positively charged bead that cannot exchange ions, the symmetry of the system breaks down and the motor is able to move with a net velocity of 3.3 μm s^{-1} for this set of parameters, with the Nafion end leading the motion. Therefore, the simulations show that this simple design of a Nafion microswimmer has the capability of self-propelling autonomously in a bulk fluid.

2.2.2 Nanofabrication strategy. In order to integrate the asymmetry in the own Nafion micro/nanostructure we have developed a cost-effective and versatile nanofabrication route based on colloidal lithography. Fig. 4 shows the different fabrication steps of the swimmers.

In brief, Nafion thin layers are spin-coated from Nafion dispersion solutions (water + low molecular weight aliphatic alcohols) onto silicon wafers coated with gold. The layer thickness is controlled by the concentration of Nafion dispersion, the spinning rate, and the number of layers deposited by repeating the spinning process. For instance, 4-micron thick layers can be deposited using 5% Nafion, with 800 rpm during one minute and repeating such a process four times.

Afterwards, the Nafion-coated wafers (which are negatively charged) are incubated with micron-sized polystyrene particles modified with amidine (conferring positive charge to the particle) to form an electrostatically self-assembled layer of particles on top. Then the samples are subjected to oxygen reactive ion etching (RIE) to define an array of micro/nanopillars using the microparticles as masks. Nafion pillar arrays of 4 μm length (including the capped

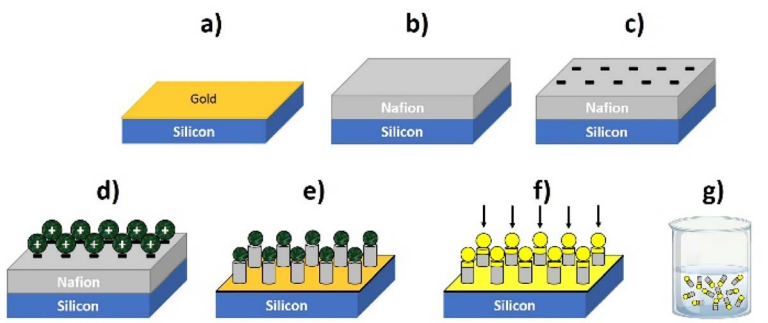

Fig. 4 Different steps in the nanofabrication process: (a) a thin layer deposition of Au on SiO_2 wafers, (b) spin coating of Nafion films (followed by heating at 100 °C for 2 minutes), (c) and (d) electrostatic self-assembly of positive colloidal particles as RIE masks taking advantage of the negative charge of Nafion films, (e) O_2 RIE to define the Nafion pillars, (f) directional metal/oxide evaporation to confer more functionality to the Nafion pillar arrays and reinforce the pillar robustness and (g) release of the Nafion structures into water with an ultrasonic bath.

particles) by 1.8 μm width are typically obtained with the following RIE conditions: 50 sccm of O_2, base pressure of 15 mTorr and HF power of 150 W for 4 minutes. The capped particles on the pillars give more asymmetry to the nanostructure to induce asymmetric gradients, an important aspect to activate their motion, as pointed out in the previous section. These arrays can be further modified by evaporating other materials on top of them, such as metals or oxides, which can also provide a suitable zeta potential to facilitate motion as well as to reinforce the Nafion/microparticle joint. In this work a thin Al_2O_3 layer has been deposited on top of the pillar to strengthen the amidine/Nafion joint. After that, the pillars can be released to a solution by sonication.

The fabrication technique exhibits versatility for motor production with respect to the motor's size, concentration and composition. Just by changing the Nafion thickness, the particle size and concentration and the evaporated material one can get a wide range of different Nafion-based motors with increased functionality. Fig. 5 shows different kinds of Nafion-based motors with different sizes and concentrations.

2.2.3 Swimming performance. The motion of these structures is activated by adding salts. In this work, 1×10^{-5} M NaCl has been used as fuel. Under these

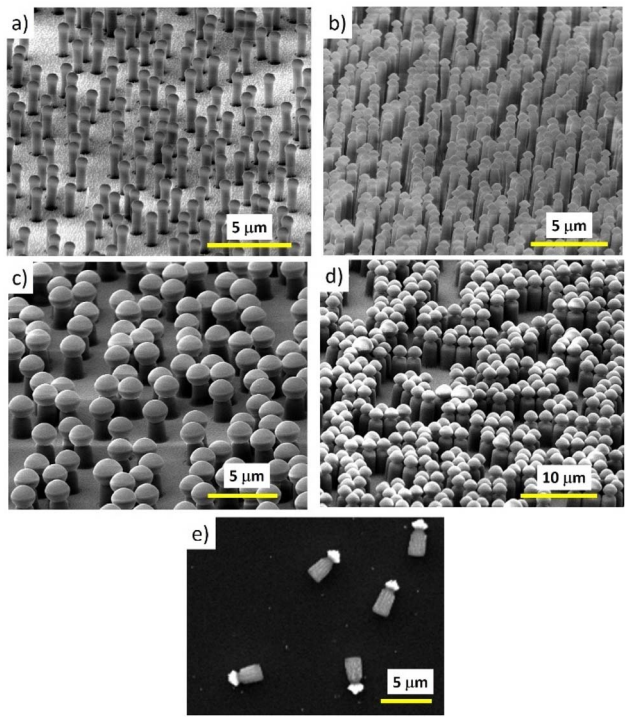

Fig. 5 Scanning electron microscope images of different Nafion arrays generated by colloidal lithography with the RIE technique. In (a) and (b) microparticles with diameters of 1 μm have been used as masks and 0.1 and 0.2% of particle dispersions, respectively. In (c) and (d) 2 μm diameter microparticles have been used as masks and 0.2% of particle dispersions but different RIE times (3 and 4 minutes, respectively). (e) Dispersed particles after an ultrasonic bath.

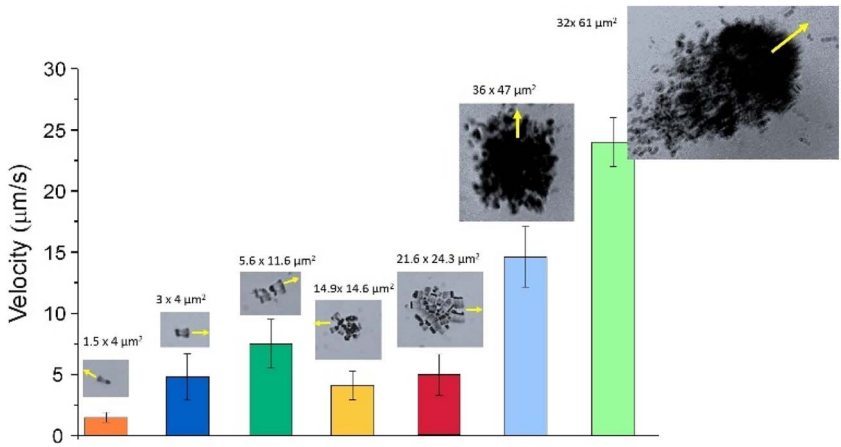

Fig. 6 Average velocity measured for individual Nafion-based swimmers and Nafion clusters of different sizes. The characteristic dimensions of the Nafion ensembles are indicated in the figure, together with the swimming direction of the collective structure.

conditions, we tracked the trajectories of individual Nafion motors and measured the average velocities (see Fig. 6 and 7). Typical individual Nafion-based microswimmers with a length of 4 μm and a width of 1.8 μm, capped with amidine particles, move with an average velocity of 1.5 μm s^{-1}. The trajectory shows directionality, with the Nafion end leading the motion as predicted by the simulations, but is largely affected by Brownian motion, showing enhanced diffusion at long times.

Clusterization of individual motors leads to enhanced velocities, a typical effect of collective behavior. Fig. 6 shows the evolution of the velocity of the Nafion structures as a function of their integration into Nafion assemblies of different sizes and shapes.

The figure shows that the velocity of two swimmers attached together is more than twice the value of the individual velocities. As the cluster grows, the velocity is enhanced especially if the resulting structure is non-symmetric. Elongated Nafion clusters seem to exhibit enhanced directional mobility compared to the more symmetric ones, with an increasing net velocity as the cluster grows in size by the incorporation of more individual Nafion swimmers.

The decay in velocity for more symmetrical clusters is illustrated in Fig. 7a with the clusters of sizes 14.9 × 14.6 μm^2 or 21.6 × 24.3 μm^2. Although they contain more active Nafion swimmers than the more elongated 5.6 × 11.6 μm^2 cluster, they propel at smaller velocities. As soon as the clusters of Nafion increase significantly in size and become a little more asymmetric, their velocities greatly speed up as observed with the clusters of sizes 36 × 47 μm^2 and 61 × 32 μm^2 which exhibited velocities of 14.6 ± 2.5 μm s^{-1} and 23.0 ± 2.0 μm s^{-1}, respectively. Therefore, small changes in symmetry result in important velocity changes since symmetric chemical gradients are needed in order to generate a net velocity. This effect can be better visualized by tracking the instantaneous velocity of a Nafion ensemble. Fig. 7a shows the change in speed of a Nafion structure as it swims. The interaction with the solvent makes its shape fluctuate from a more

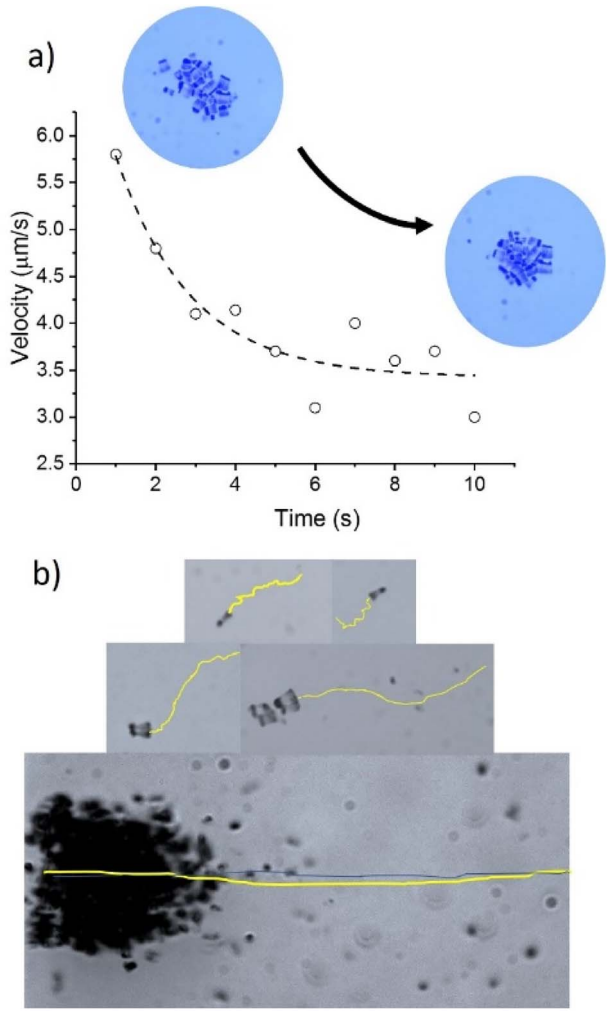

Fig. 7 (a) Velocity profile as a function of time together with the shape changes of the cluster by solvent-induced fluctuations. (b) Trajectories of the Nafion objects as function of their cluster size.

elongated towards a more symmetrical shape with the consequent velocity decrease from around 6 to below 4 μm s^{-1}. The impact of shape fluctuations is also reflected in the standard deviation of the average velocities. The large error bars in the cluster velocities in Fig. 6 can partially be ascribed to changes in their shape during swimming. Individual swimmers and clusters with decreased velocities are more affected by Brownian motion resulting in more zigzagging trajectories. However, as the velocity of the ensembles increases, the trajectories become more directional, as represented in Fig. 7b.

The formation of Nafion swimmer ensembles mainly occurs due to the fluid pumping capabilities of the structures. These assemblies behave as mobile pumps, dragging fluid towards them and attracting objects nearby. During the initial stages of cluster formation, individual Nafion swimmers approach each

other enhanced by their active motion. As soon as a few Nafion swimmers are brought together, the resulting Nafion cluster starts to efficiently pump fluid, dragging more active objects along with it, which in turn increases the pumping performance as the cluster grows in size. For instance, small clusters of 14.9 × 14.6 μm^2 or 21.6 × 24.3 μm^2 can pump fluid and objects at velocities around 4–7 $\mu m\ s^{-1}$. As the cluster size increases, such as the one shown in Fig. 8a with dimensions of 60 × 32 μm^2, the average pumping velocity can increase up to 33.6 ± 3.4 $\mu m\ s^{-1}$. The figure shows a cluster of Nafion objects swimming and simultaneously collecting the nano-objects nearby. The trajectories of Nafion objects pumped towards the big cluster are shown in yellow lines. The figure also collects the velocities of a couple of individual nano-objects pumped to the big cluster as a function of the radial distance (Fig. 8b). Note that the radial distance of 35 μm almost coincides with the border of the motile Nafion cluster, exhibiting the highest fluid pumping velocity at such distance (see the video in the ESI†).

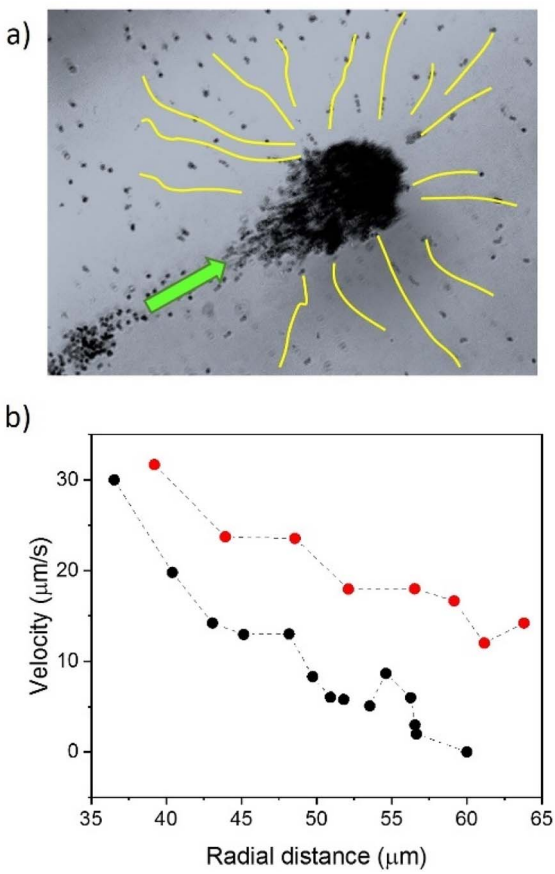

Fig. 8 (a) A big cluster of Nafion swimmers moving at high velocity and pumping nearby objects while swimming. The attraction of objects towards the mobile pump is illustrated by the trajectories of nearby individual swimmers, represented by the yellow solid lines. (b) Velocity of two of these nearby individual Nafion swimmers attracted by the big swimming cluster as a function of the radial distance to the cluster.

3. Conclusions

We have designed asymmetric Nafion-based nanostructures which can move by themselves triggered by the ion-exchange process with salt cations contained in the aqueous solution in which they are immersed. Such nanostructures have been fabricated through a versatile strategy based on colloidal lithography. The resulting Nafion swimmers can efficiently interact with other swimmers nearby favored by their active motion and self-assemble to form motile clusters promoted by their self-generated chemical gradients and local electric field. The swimming velocity of clusters increases as the cluster size increases and becomes more asymmetric reaching values above 20 μm s^{-1}. Such clusters behave as powerful mobile pumps attracting objects close by at high pumping velocities (around 30 μm s^{-1}) while swimming. Such collective behaviour together with the versatility of the fabrication routes can be exploited to promote cooperative and efficient motor functionalities. However, there are still many fundamental issues to be addressed, especially in the details of the interaction process and clusterization or in the impact of walls or zeta potential of the passive cap. Nevertheless, these results encourage us to continue investing efforts in the fundamental understanding of these fascinating systems in order to optimize and create innovative applications specially in the area of environmental remediation. By leveraging these collective interactions, microswimmers could effectively capture and remove a wide range of contaminants, including pollutants, bacteria, and even microplastics, from a fluid medium. Furthermore, they possess the additional advantage of being easily collected through appropriate functionalization and are recyclable.

Author contributions

M. J. E., D. R. and J. F. conceived the work. M. J. E. and D. R. designed the experiments. M. J. E. performed the experiments and analysed the data.

Conflicts of interest

There are no conflicts to declare.

Acknowledgements

This research was supported by the Spanish Ministry of Science and Innovation (MCIN) under Contracts No. PID2021-124568NB-I00 and PID2021-126570NB-I00. The ICN2 is funded by the CERCA program/Generalitat de Catalunya. The ICN2 is supported by the Severo Ochoa Centres of Excellence programme, Grant CEX2021-001214-S, funded by MCIN/AEI/10.13039.501100011033. We also acknowledge the scientific exchange and support of the Centre for Molecular Water Science (CMWS).

Notes and references

1 W. Wang, W. Duan, S. Ahmed, T. E. Mallouk and A. Sen, *Nano Today*, 2013, **8**, 531–554.

2 V. Yadav, W. Duan, P. J. Butler and A. Sen, *Annu. Rev. Biophys.*, 2015, **44**, 77–100.
3 A. Somasundar and A. Sen, *Small*, 2021, **17**, 2007102.
4 P. L. Venugopalan, B. Esteban-Fernández De Ávila, M. Pal, A. Ghosh and J. Wang, *ACS Nano*, 2020, **14**, 9423–9439.
5 J. Yong, A. S. Mellick, J. Whitelock, J. Wang and K. Liang, *Adv. Mater.*, 2023, **35**, 2205746.
6 M. Urso, M. Ussia and M. Pumera, *Nat. Rev. Bioeng.*, 2023, **1**, 236–251.
7 J. Parmar, D. Vilela, K. Villa, J. Wang and S. Sánchez, *J. Am. Chem. Soc.*, 2018, **140**, 9317–9331.
8 B. Jurado-Sánchez and J. Wang, *Environ. Sci.: Nano*, 2018, **5**, 1530.
9 J. Li, B. Esteban-Fernández de Ávila, W. Gao, L. Zhang and J. Wang, *Sci. Rob.*, 2017, **2**, eaam6431.
10 B. E.-F. de Ávila, P. Angsantikul, J. Li, M. Angel Lopez-Ramirez, D. E. Ramírez-Herrera, S. Thamphiwatana, C. Chen, J. Delezuk, R. Samakapiruk, V. Ramez, M. Obonyo, L. Zhang and J. Wang, *Nat. Commun.*, 2017, **8**, 272.
11 W. Duan, W. Wang, S. Das, V. Yadav, T. E. Mallouk and A. Sen, *Annu. Rev. Anal. Chem.*, 2015, **8**, 311–333.
12 M. Pacheco, M. A. López, B. Jurado-Sánchez, *et al.*, *Anal. Bioanal. Chem.*, 2019, **411**, 6561–6573.
13 G. Gompper, R. G. Winkler, T. Speck, *et al.*, *J. Phys.: Condens. Matter*, 2020, **32**, 193001.
14 P. Illien, R. Golestanian and A. Sen, *Chem. Soc. Rev.*, 2017, **46**, 5508–5518.
15 K. Gentile, A. Somasundar, A. Bhide and A. Sen, *Chem*, 2020, **6**, 2174–2185.
16 R. Wu, Y. Zhu, X. Cai, S. Wu, L. Xu and T. Yu, *Micromachines*, 2022, **13**, 1473.
17 F. Ji, Y. Wu, M. Pumera and L. Zhang, *Adv. Mater.*, 2023, **35**, 1–42.
18 J. C. Fraire, M. Guix, A. C. Hortelao, N. Ruiz-González, A. C. Bakenecker, P. Ramezani, C. Hinnekens, F. Sauvage, S. C. De Smedt, K. Braeckmans and S. Sánchez, *ACS Nano*, 2023, **17**, 7180–7193.
19 A. C. Hortelao, C. Simó, M. Guix, S. Guallar-Garrido, E. Julián, D. Vilela, L. Rejc, P. Ramos-Cabrer, U. Cossío, V. Gómez-Vallejo, T. Patiño, J. Llop and S. Sánchez, *Sci. Rob.*, 2021, **6**, eabd2823.
20 K. K. Dey, F. Wong, A. Altemose and A. Sen, *Curr. Opin. Colloid Interface Sci.*, 2016, **21**, 4–13.
21 W. Wang, W. Duan, S. Ahmed, A. Sen and T. E. Mallouk, *Acc. Chem. Res.*, 2015, **48**, 1938–1946.
22 A. A. Farniya, M. J. Esplandiu, D. Reguera and A. Bachtold, *Phys. Rev. Lett.*, 2013, **111**, 168301.
23 K. Zhang, J. Fraxedas, B. Sepulveda and M. J. Esplandiu, *ACS Appl. Mater. Interfaces*, 2017, **9**, 44948–44953.
24 M. J. Esplandiu, A. Afshar Farniya and A. Bachtold, *ACS Nano*, 2015, **9**, 11234–11240.
25 M. J. Esplandiu, K. Zhang, J. Fraxedas, B. Sepulveda and D. Reguera, *Acc. Chem. Res.*, 2018, **51**, 1921–1930.
26 M. J. Esplandiu, A. Afshar Farniya and D. Reguera, *J. Chem. Phys.*, 2016, **144**, 124702.
27 S. Sanchez, L. Soler and J. Katuri, *Angew. Chem., Int. Ed.*, 2015, **54**, 1414–1444.
28 M. J. Esplandiu, D. Reguera, D. Romero-Guzmán, A. M. Gallardo-Moreno and J. Fraxedas, *Nat. Commun.*, 2022, **13**, 2812.

29 K. A. Mauritz and R. B. Moore, *Chem. Rev.*, 2004, **104**, 4535–4586.
30 B. Chai, H. Yoo and G. H. Pollack, *J. Phys. Chem. B*, 2009, **113**, 13953–13958.
31 J. M. Schurr, B. S. Fujimoto, L. Huynh and D. T. Chiu, *J. Phys. Chem. B*, 2013, **117**, 7626–7652.
32 D. Florea, S. Musa, J. M. R. Huyghe and H. M. Wyss, *Proc. Natl. Acad. Sci. U. S. A.*, 2014, **111**, 6554–6559.
33 M. J. Esplandiu, D. Reguera and J. Fraxedas, *Soft Matter*, 2020, **16**, 3717–3726.
34 A. Reinmüller, H. J. Schöpe and T. Palberg, *Langmuir*, 2013, **29**, 1738–1742.
35 R. Niu, D. Botin, J. Weber, A. Reinmüller and T. Palberg, *Langmuir*, 2017, **33**, 3450–3457.
36 R. Niu and T. Palberg, *Soft Matter*, 2018, **14**, 7554–7568.
37 C. Wu, J. Dai, X. Li, L. Gao, J. Wang, J. Liu, J. Zheng, X. Zhan, J. Chen, X. Cheng, M. Yang and J. Tang, *Nat. Nanotechnol.*, 2021, **16**, 288–295.